Molecular Physics
Vol. 110, Nos. 11–12, 10–20 June 2012, 1189–1203

Taylor & Francis
Taylor & Francis Group

INVITED ARTICLE

SAFT-γ force field for the simulation of molecular fluids: 3. Coarse-grained models of benzene and hetero-group models of *n*-decylbenzene

Thomas Lafitte†, Carlos Avendaño‡, Vasileios Papaioannou, Amparo Galindo, Claire S. Adjiman, George Jackson and Erich A. Müller*

Department of Chemical Engineering, Centre for Process Systems Engineering, Imperial College London, South Kensington Campus, London SW7 2AZ, UK

(*Received 30 November 2011; final version received 23 January 2012*)

In the first paper of this series [C. Avendaño, T. Lafitte, A. Galindo, C.S. Adjiman, G. Jackson, and E.A. Müller, J. Phys. Chem. B **115**, 11154 (2011)] our methodology for the development of accurate coarse-grained (CG) SAFT-γ force fields for the computer simulation of molecular fluids was introduced with carbon dioxide as a particular case study. The procedure involves the use of a molecular-based equation of state to obtain effective intermolecular parameters (from experimental fluid phase equilibrium data) appropriate for molecular simulation over a wide range of fluid conditions. We now extend the methodology to develop coarse-grained models for benzene (C_6H_6) that can be used in fluid phase simulations. Our SAFT-γ CG force fields for benzene consist of a simple single-segment spherical model, and a rigid three-segment ring structure of tangent spherical groups interacting via Mie (generalized Lennard-Jones) segment–segment interactions. The description of the fluid phase behaviour of benzene with our simplified CG force fields is found to be comparable to that obtained with the more sophisticated models commonly used in the field; a marked improvement is seen with our SAFT-γ models for the vapour pressure, particularly at lower temperatures. These models of benzene together with the previously developed SAFT-γ three-segment chain model of *n*-decane are used to develop hetero-group force fields for *n*-decylbenzene, in the spirit of a group contribution methodology. In our approach, the parameters of the phenyl and *n*-decyl groups are obtained transferably from the individual models of benzene and *n*-decane, respectively, and the unlike energetic parameters between the phenyl and decyl segments can be obtained from vapour–liquid equilibria data for *n*-decylbenzene using the SAFT-γ equation of state. The resulting CG hetero-group models are found to describe the fluid properties of *n*-decylbenzene over a wide range of conditions, exemplifying how our approach can be used as a group contribution methodology. This is the first example of the development of hetero-group SAFT-γ force fields for molecules formed from Mie segments of different size, energy, softness/hardness, and range.

Keywords: SAFT; force field; MD; potentials; simulations

1. Introduction

Many interesting and important phenomena in soft matter, such as self-assembly of large complex molecules, protein folding or colloidal aggregation, are typically observed in the mesoscale regime. The spatial and time scales involved in these processes are very large, making atomistic simulations very challenging. The growing area of coarse graining (CG) has made it possible to use conventional molecular simulation techniques to study large systems in a reasonable computing time [1,2]. In generic CG methodologies, molecules are described as being formed from segments of bundles of matter (super-atoms) interacting via effective CG potentials. This approach clearly involves a loss in chemical resolution of the description of the system, hence it is important to have an appropriate methodology that preserves a good overall description of the key target properties that one wants to represent after the coarse graining.

A variety of CG approaches have been proposed in recent years. Excellent reviews describing advances in CG methods can be found in the literature [3–8]. Most of these methodologies employ a 'bottom-up' scheme, in which an accurate and detailed description of the thermodynamic and/or structural properties of the system is used in order to develop the CG models. These properties are often calculated at the atomistic or quantum-mechanical level of resolution, which makes the approaches very time consuming.

*Corresponding author. Email: e.muller@imperial.ac.uk
†Present address: Department of Chemical Engineering, Princeton University, Princeton, New Jersey 08544, USA.
‡Present address: School of Chemical and Biomolecular Engineering, Cornell University, Ithaca, New York 14853, USA.

ISSN 0026–8976 print/ISSN 1362–3028 online

http://dx.doi.org/10.1080/00268976.2012.662303
http://www.tandfonline.com

Two common methodologies which make use of this procedure are iterative Boltzmann inversion [3,9,10] and force-matching methods [1,7,11–13]. By contrast, with 'top-down' approaches macroscopic experimental data are used to construct the CG molecular models; in this case a model is proposed and the molecular parameters are modified in a systematic way until one or more of the macroscopic properties are reproduced. Typical examples of models developed with this type of 'top-down' approach include the MARTINI force field [14], and the force fields introduced by Klein and co-workers [15–18]. An important difference between these two force fields is the functional form chosen for the dispersion interactions between the segments making up the molecules: the former is based on a simple Lennard-Jones (LJ) 12–6 potential [19,20], while the latter makes use of the more general Mie (generalized Lennard-Jones) potential [21]. Maerzke and Siepmann [22] have also applied the Mie potential to describe the inter-segment interactions of molecules formed from CG Mie segments, where the models are developed specifically for use in representing phase equilibria.

Recently, we introduced a coarse-graining methodology, where a molecular-based equation of state (EoS) of the statistical associating fluid theory (SAFT) family [23,24] is used as the link between the experimental fluid phase equilibria data and novel CG force fields based on the Mie potential [25,26], thereby facilitating parameterization. Details of the various incarnations of the SAFT EoS and examples of the successful application of the approach in the description of the fluid-phase behaviour and other thermodynamic properties for a broad variety of systems can be found in [27–30]. In our current work we use a recent reformulation of the theory for potential of variable range (SAFT-VR). The SAFT-VR approach was originally developed to describe chain molecules formed from square-well, Yukawa, or Lennard-Jones segments [31–34], and later extended to the Mie potential [35,36]. The Mie [21] potential is expressed in terms of two exponents λ_r and λ_a (which characterize the softness/hardness of the repulsion and the range of the attractive interaction, respectively) as

$$u^{\mathrm{Mie}}(r) = \mathcal{C}\epsilon\left[\left(\frac{\sigma}{r}\right)^{\lambda_r} - \left(\frac{\sigma}{r}\right)^{\lambda_a}\right], \tag{1}$$

where r is the intersegment distance, ϵ is the potential well depth, σ is the segment diameter, and $\mathcal{C}$ is given by

$$\mathcal{C} = \frac{\lambda_r}{\lambda_r - \lambda_a}\left(\frac{\lambda_r}{\lambda_a}\right)^{\lambda_a/(\lambda_r-\lambda_a)} \tag{2}$$

to ensure that the minimum of the potential is $-\epsilon$. The latest enhanced version of the SAFT-VR EoS [36] provides an improved description of the near-critical fluid region for chains of Mie segments that is accurate for a wide range of repulsive and attractive exponents. The Mie potential is more versatile than the Lennard-Jones 12–6 potential as both the repulsions and the range of the attractions between segments can be tuned separately. In this paper we refer to the latest version of the theory as SAFT-VR Mie [36] and the coarse-grained models generated with it as the SAFT-γ CG force field. Here, SAFT-γ denotes the more generic group-contribution reformulation of the EoS for heteronuclear molecules formed from fused segments of different type (size and interactions) [37–40]; in this case the separate contributions to the Helmholtz free energy are expressed as appropriate functions of the parameters and numbers of different segments representing the chemical groups making up the molecules.

Our CG methodology has already been applied to describe the fluid-phase thermophysical properties of green-house molecules such as CO_2, CF_4, and SF_6, and long-chain alkanes, *n*-decane and *n*-eicosane [25,26]. The SAFT-y CG force fields are found to provide a comparable description of the fluid phase equilibria to the more sophisticated models commonly used in molecular simulation at a fraction of the computational cost. In the current work we extend and further apply this methodology to obtain CG models of benzene and alkylbenzenes. Benzene and other aromatic compounds are important not only in the chemical industry, but also in biological science, as aromatic groups are often found in biomolecules. The nature of π–π interactions in aromatic molecules is not simple to represent, leading to a non-trivial potential energy landscape [41,42]. Hunter and Sanders [41] have developed a model to describe π–π forces, in terms of key contributions, namely, the electrostatic, inductive, dispersive, and repulsive interactions. The reader is directed to the excellent review by Hunter *et al*. [42] for a relatively recent account. It is clear that in order to obtain an appropriate CG model for aromatic molecules these contributions should be included in an effective manner within the intermolecular force field.

Here, we develop an effective CG model of benzene which incorporates the average effective interactions by means of the softness/hardness and range parameters of the Mie potential which are parameterized to reproduce the fluid phase behaviour of benzene over a wide range of thermodynamic conditions. Two different models for benzene are considered as shown in Figure 1: a simple single-segment spherical model [Figure 1(a)], and a rigid tangent three-segment ring structure [Figure 1(b)]. Although the simple spherical model may at first glance appear to be a gross

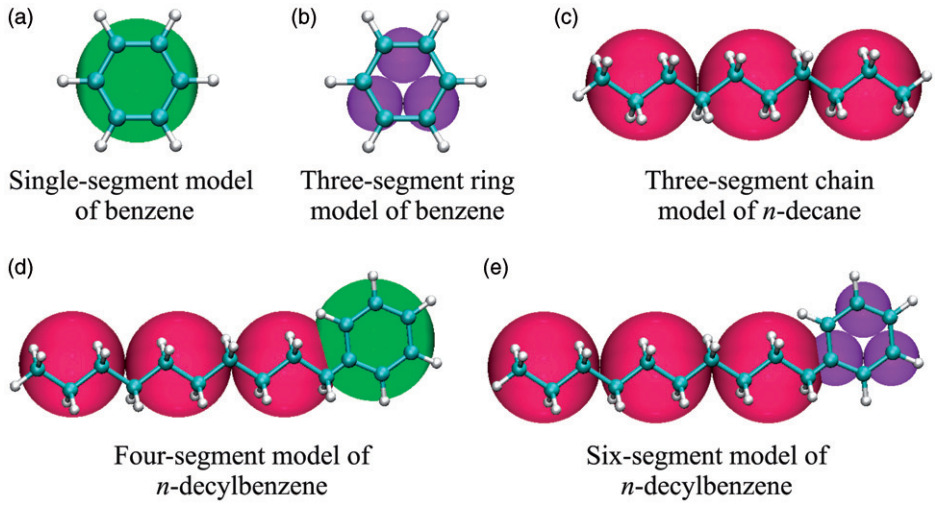

Figure 1. Schematic representation of the SAFT-γ CG models used in this work. The models presented are: (a) the single-segment spherical model and (b) three-segment ring model of benzene; (c) the three-segment chain model of *n*-decane; (d) the four-segment model of *n*-decylbenzene constructed using the single-segment model of benzene and the three-segment chain model of *n*-decane; (e) six-segment model of *n*-decylbenzene constructed using the three-segment ring model of benzene and the three-segment chain model of *n*-decane.

oversimplification of the benzene molecule, we will show that it can be used to provide a good representation of the fluid phase behaviour, particularly away from the critical point. The three-segment ring model of benzene is found to be superior in describing the coexistence properties of benzene over the temperature range explored, and provides an equivalent description to that obtained with more sophisticated models such as the OPLS [43,44] or TraPPE six-segment united-atom (UA) force fields. Although the computational cost of simulations with a three-segment model is an order of magnitude higher than with a simple spherical model, it still offers a significant saving compared with the united-atom and atomistic models. A single-segment model is recommended for fast calculations of the fluid phase equilibria of benzene. For properties where the planar structure of the aromatic ring is important, a ring model of benzene is clearly preferable.

Zacharopoulos *et al.* [45] have proposed a CG method for the description of the nonbonded interactions between benzene molecules based on the interactions between pairs of moieties with reduced degrees of freedom (in this case down to four or six dimensions) from tabulated values of the energy of a fully atomistic representation obtained with the COMPASS [46] force field. The thermodynamic properties (pressure and internal energy) and more particularly the structure obtained with their CG model is found to be in very good agreement with the atomistic representation. A three-segment ring model has been used in the development of the MARTINI force field [14], where three fused Lennard-Jones segments are used to describe the planar structure of benzene. More recently, DeVane *et al.* [47] have proposed a four-segment ring model of benzene comprising groups interacting via the Mie potential. The intramolecular interactions used in their model were determined using *ab initio* calculations; ultimately the molecules were found to behave as essentially rigid (inflexible) structures. The inter-segment parameters of their model were then refined to reproduce the surface tension and liquid density of benzene for a single simulated thermodynamic state. An advantage of our approach is that our algebraic SAFT-VR Mie EoS accurately describes the thermodynamic properties of molecules formed from Mie segments, and thus allows a rapid estimation of the effective force-field parameters which are applicable for simulations over a wide range of conditions.

2. SAFT-γ coarse-graining methodology

The SAFT-γ CG methodology [25,26] is based on using an accurate algebraic EoS as the link between the experimental fluid phase equilibria and the parameters of CG models for use in molecular simulation. The advantages of our SAFT-γ CG approach are twofold. Firstly, this 'top-down' methodology allows one to overcome the heavy computational burden usually associated with the determination of intermolecular parameters that provide an accurate description of the experimental data over a broad range of thermodynamic conditions. The second benefit lies in the flexibility of the Mie-based SAFT-γ force fields,

which enable one to explore widely differing forms of intermolecular potential by varying the hardness/softness of the repulsion and the range of attraction between segments.

2.1. *CG models formed from identical Mie segments*

A SAFT description is invariably based on the Wertheim [48–51] first-order thermodynamic perturbation theory (TPT1) for associating fluids where the general formulation of the Helmholtz free energy A for N non-associating chains formed from m_s monomeric segments can be expressed in terms of separate contributions as

$$a = a^{\mathrm{IDEAL}} + a^{\mathrm{MONO}} + a^{\mathrm{CHAIN}}. \tag{3}$$

Here, $a = A/(Nk_BT)$ is the dimensionless Helmholtz free energy, a^{IDEAL} is the ideal contribution, a^{MONO} is the contribution due to the monomer segments, a^{CHAIN} is the contribution due to the formation of the chains of segments, T is the temperature, and k_B is the Boltzmann constant. In most applications, one considers chains of linearly bonded segments. For chains of m_s tangentially bonded Mie segments of the same type, one can employ the linear approximation for the m_s-body correlation function to express the contribution to the free energy due to chain formation as [52,53]

$$a^{\mathrm{CHAIN}} = -(m_s - 1)\ln g^{\mathrm{Mie}}(\sigma), \tag{4}$$

where $g^{\mathrm{Mie}}(\sigma)$ is the contact value of the radial pair distribution function for the reference monomeric Mie fluid [36].

The corresponding expression for rings formed from m_s tangentially bonded segments can also easily be derived [54–57]. The basic idea is to assume that the difference between a chain and a ring molecule of the same length is that the latter has an extra bond. It is then possible to obtain the underlying reduction in free energy of forming the ring structure solely in terms of the contact value of the pair distribution function of the reference non-bonded system. The contribution due to the formation of an m_s-membered ring of tangent Mie segments can then be written simply as [54]

$$a^{\mathrm{RING}} = -m_s \ln g^{\mathrm{Mie}}(\sigma). \tag{5}$$

The ring contribution, Equation (5), can then be used instead of the chain contribution in Equation (3) to provide an EoS for molecules formed from rings of tangent Mie segments of the same type.

In common with other analytical statistical mechanical approaches for complex fluids, a number of approximations have to be made in the development of the SAFT-VR Mie EoS [36] and related approaches. This means, of course, that the theoretical description will not provide a perfect match to the 'exact' numerical results of molecular simulation for a given intermolecular potential model. In the case of small spherical or near-spherical molecules the SAFT-VR Mie description is very accurate, and the agreement with simulation is good enough to develop high fidelity force fields. For longer chain molecules or ring structures an additional refinement scheme can be used to eliminate the possible discrepancy between the EoS calculations and the simulation data. This single-step refinement procedure (cf. stage iii below) was described in the context of the development of SAFT-γ CG force fields for *n*-decane and *n*-eicosane modelled as chains of Mie segments [26]. Van Westen *et al.* [58] have used an iterative procedure to obtain TraPPE-like force fields for alkanes modelled as LJ chains based on the PC-SAFT EoS; however, because of the blurring of the link between the precise intermolecular potential and the PC-SAFT description, a number of additional simulations had to be performed for each set of parameters to obtain a reliable model. The specific details of our procedure for the estimation of the force-field parameters are exemplified here in the particular case of the development of SAFT-γ CG models for benzene:

(i) First, the relative least-squares residuals between the experimental and estimated (via the EoS) values of the vapour pressure P_v and saturated liquid densities ρ_l are minimized for a broad range of temperatures. If one assumes that benzene can be represented as a single-segment spherical model ($m_s = 1$) or three-segment ring structure ($m_s = 3$), then the number of segments m_s is no longer an estimation parameter and the corresponding objective function F can be written as

$$\begin{aligned}
&\min_{\sigma^{\mathrm{SAFT}},\epsilon^{\mathrm{SAFT}},\lambda_r^{\mathrm{SAFT}},\lambda_a^{\mathrm{SAFT}}} F_{\exp}(\sigma^{\mathrm{SAFT}},\epsilon^{\mathrm{SAFT}},\lambda_r^{\mathrm{SAFT}},\lambda_a^{\mathrm{SAFT}}) \\
&= \min_{\sigma^{\mathrm{SAFT}},\epsilon^{\mathrm{SAFT}},\lambda_r^{\mathrm{SAFT}},\lambda_a^{\mathrm{SAFT}}} \left\{ \sum_{i=1}^{N_P} \left[\frac{\left\{ \begin{array}{c} P_v^{\exp}(T_i) - \\ P_v^{\mathrm{SAFT}}(T_i;\sigma^{\mathrm{SAFT}},\epsilon^{\mathrm{SAFT}}, \\ \lambda_r^{\mathrm{SAFT}},\lambda_a^{\mathrm{SAFT}}) \end{array} \right\}}{P_v^{\exp}(T_i)} \right]^2 \right. \\
&\left. + \sum_{j=1}^{N_\rho} \left[\frac{\left\{ \begin{array}{l} \rho_l^{\exp}(T_j) - \\ \rho_l^{\mathrm{SAFT}}(T_j;\sigma^{\mathrm{SAFT}},\epsilon^{\mathrm{SAFT}},\lambda_r^{\mathrm{SAFT}},\lambda_a^{\mathrm{SAFT}}) \end{array} \right\}}{\rho_l^{\exp}(T_j)} \right]^2 \right\},
\end{aligned} \tag{6}$$

where N_p and N_ρ are the number of experimental points for the vapour pressure ($P_v^{\exp}$)

and saturated liquid density ($\rho_l^{\text{exp}} = N_l/V$), respectively. The experimental data for benzene are obtained from the NIST database [59]. This allows us to estimate the SAFT-VR Mie parameters σ^{SAFT}, ϵ^{SAFT}, $\lambda_{\text{r}}^{\text{SAFT}}$, $\lambda_{\text{a}}^{\text{SAFT}}$ which provide the optimal description of the experimental data.

(ii) The vapour pressure and saturated liquid density are then computed by numerical (in our case molecular dynamics) simulation for selected states using the parameters $\sigma^{\text{SAFT}}, \epsilon^{\text{SAFT}}, \lambda_{\text{r}}^{\text{SAFT}}, \lambda_{\text{a}}^{\text{SAFT}}$ obtained from the optimization in stage (i) (and the specified m_{s}).

(iii) Due to the approximations employed in the theory, one will typically find discrepancies between the calculated values and the molecular simulation results. As a result, the optimal parameters for use in molecular simulation may differ from those obtained directly from the equation of state. In order to find the optimal values $\sigma^{\text{sim}}, \epsilon^{\text{sim}}, \lambda_{\text{r}}^{\text{sim}}, \lambda_{\text{a}}^{\text{sim}}$ for use in simulation, we make use of a corresponding state procedure. For this purpose, we assume that the optimal non-conformal parameters $\lambda_{\text{r}}^{\text{SAFT}}$ and $\lambda_{\text{a}}^{\text{SAFT}}$ are the same in both the equation of state and the molecular simulation so that only the size and energy parameters σ^{sim} and ϵ^{sim} need to be refined. These can easily be obtained with a procedure which is similar to the recursive scheme reported by van Westen *et al*. [58]. In the same spirit we first define two correction constants c_σ, and c_ϵ which relate the SAFT parameters σ^{SAFT} and ϵ^{SAFT} to the scaled parameters σ^{scaled} and ϵ^{scaled}:

$$\sigma^{\text{scaled}} = c_\sigma \sigma^{\text{SAFT}}, \tag{7a}$$

$$\epsilon^{\text{scaled}} = c_\epsilon \epsilon^{\text{SAFT}}. \tag{7b}$$

As the key step of our refinement procedure, the scaled size σ^{scaled} and energy ϵ^{scaled} parameters are obtained by minimizing the following objective function:

$$\begin{aligned}\min_{\sigma^{\text{scaled}},\epsilon^{\text{scaled}}} F_{sim}(\sigma^{\text{scaled}},\epsilon^{\text{scaled}}) &= \min_{\sigma^{\text{scaled}},\epsilon^{\text{scaled}}} \left\{ \sum_{i=1}^{N_P^{\text{sim}}} \left[\frac{\left\{ P_{\text{v}}^{\text{sim}}(T_i;\sigma^{\text{SAFT}},\epsilon^{\text{SAFT}}) - P_{\text{v}}^{\text{SAFT}}(T_i;\sigma^{\text{scaled}},\epsilon^{\text{scaled}}) \right\}}{P_v^{\text{sim}}(T_i;\sigma^{\text{SAFT}},\epsilon^{\text{SAFT}})} \right]^2 \right. \\ &\left. + \sum_{j=1}^{N_\rho^{\text{sim}}} \left[\frac{\left\{ \rho_l^{\text{sim}}(T_j;\sigma^{\text{SAFT}},\epsilon^{\text{SAFT}}) - \rho_l^{\text{SAFT}}(T_j;\sigma^{\text{scaled}},\epsilon^{\text{scaled}}) \right\}}{\rho_l^{\text{sim}}(T_j;\sigma^{\text{SAFT}},\epsilon^{\text{SAFT}})} \right]^2 \right\}, \end{aligned} \tag{8}$$

where $P_{\text{v}}^{\text{sim}}$ and ρ_l^{sim} are the vapour pressure and saturated liquid density obtained by molecular simulation in stage (ii); the sums are now over the simulated data points, N_P^{sim} for the vapour pressure and N_ρ^{sim} for the saturated liquid density.

(iv) Having determined the correction constants $c_\sigma = \sigma^{\text{scaled}}/\sigma^{\text{SAFT}}$, and $c_\epsilon = \epsilon^{\text{scaled}}/\epsilon^{\text{SAFT}}$, it is then straightforward to determine a refined set of parameters σ^{sim} and ϵ^{sim} for use in simulation to provide an improved description of the fluid phase equilibria of the system. Since the repulsive and attractive exponents are fixed we have a conformal fluid, and the parameter space can be rescaled so that the refined values are simply obtained from

$$\sigma^{\text{sim}} = \sigma^{\text{SAFT}}/c_\sigma, \tag{9a}$$

$$\epsilon^{\text{sim}} = \epsilon^{\text{SAFT}}/c_\epsilon. \tag{9b}$$

One should note that an advantage of this scheme is that it does not involve an iterative simulation procedure. As a set of molecular simulations would in any case be performed to assess the adequacy of the SAFT-γ force field obtained in stage (i), the determination of the optimal parameter set can be obtained without the need for additional simulations.

The molecular parameters for benzene obtained in this way for our single-segment and three-segment ring SAFT-γ CG force fields are reported in Table 1. As well as the final set of model parameters recommended for use in molecular simulations of fluid benzene, we report for comparison the parameters obtained after the first estimation procedure [stage (i)] using the SAFT-VR Mie EoS and the experimental data. In all of these models the attractive exponent characterizing the CG Mie segments is fixed to the London [60] dispersion value of $\lambda_{\text{a}} = 6$ to reduce the number of adjustable parameters. The same refinement procedure was used to develop accurate SAFT-γ CG force fields for the fluid phase equilibria and other thermodynamic properties of *n*-decane and *n*-eicosane in previous work [26]. The refined parameters for *n*-decane modelled as a linear chain of three tangent Mie segments are also given in Table 1 for completeness.

2.2. *CG models formed from different Mie segments*

As an example of the versatility of our approach we present a preliminary extension of the methodology to develop a hetero-group model of *n*-decylbenzene. Although a full discussion of the generalization of the SAFT EoS to heteronuclear molecules formed

Table 1. Optimized SAFT-γ CG Mie force fields for the molecules studied in our work. The five parameters that characterize the models are: the number of segments per molecule m_s, the Mie potential energy well depth ϵ, the diameter of the segment σ, and the repulsive and attractive Mie exponents, λ_r and λ_a, respectively. The parameters obtained directly from the initial estimation using the SAFT-VR Mie EoS (σ^{SAFT}, ϵ^{SAFT}), and the refined parameters obtained after using the procedure outlined in Section 2.1 (σ^{sim}, ϵ^{sim}) are presented. The ring and chain structures are formed from tangentially bonded segments, i.e. the distance between segments is the diameter of the segment itself. The attractive exponent λ_a is set to the London dispersion value for all of these models.

molecule	m_s	σ^{SAFT}	ϵ^{SAFT}/k_B	σ^{sim}	ϵ^{sim}/k_B	λ_r	λ_a
benzene	1	5.293 Å	658.17 K	5.293 Å	658.17 K	32.00	6.00
benzene	3 (ring)	3.482 Å	243.88 K	3.490 Å	258.28 K	11.58	6.00
n-decane	3 (chain)	4.603 Å	407.09 K	4.629 Å	414.90 K	19.61	6.00

from segments of different type is beyond the scope of the current paper, we give a brief account of the key developments. The Wertheim TPT1 approach has been extended to treat purely repulsive heteronuclear molecules formed from hard sphere segments of different diameter; the resulting bonded-hard sphere (BHS) theory has been shown to describe accurately the equation of state of hard multifunctional molecules with segments that are either tangentially bonded [54,61–63] or in a fused configuration [64]. Heteronuclear versions of the SAFT equation of state have also been developed for attractive van der Waals [65], square-well [66–70], and Lennard-Jones [71–74] segments. The version of the SAFT-VR theory for molecules formed from different square-well segments has been the basis for group contribution extensions of the approach such as GC-SAFT-VR [75,76] and SAFT-γ [37–39]. The latest version of the SAFT-γ EoS formulated for molecules formed from Mie segments of different type [40] is employed in our current paper to aid in the development of a hetero-group SAFT-γ force field for *n*-decylbenzene.

In the usual group contribution spirit, the *n*-decylbenzene molecule can be represented by combining the models obtained for benzene and the *n*-decane chain [see Figures 1(d)–(e)]. Our simplest force field is constructed by using the single-segment model of benzene together with the three-segment chain model of *n*-decane. These models are fused together as the first example of the development of a hetero-group force field using the SAFT-γ CG methodology. The unlike attractive interactions between the *n*-decane and the benzene Mie segments are obtained with the SAFT-γ Mie EoS [40] by transferring the like parameters of the models for benzene and *n*-decane, while the unlike benzene–alkane segment–segment interaction is estimated from the fluid-phase equilibria of pure *n*-decylbenzene. All of the segment–segment parameters necessary for the characterization of this model of *n*-decylbenzene are summarized in Table 2; we also include expressions of the simple combining rules used for the unlike segment size and repulsive exponent of the Mie interactions. In order to account for the covalent bond between the aromatic (phenyl) and aliphatic groups (*n*-decyl), the two models are fused as shown in Figure 1(d), i.e., the benzene segment and the first segment of the *n*-decane model are not considered to be bonded tangentially. As we do not yet have a precise mapping procedure for the development of the parameters of fused hetero-group models with the SAFT-γ approach, the optimal bond length is obtained by performing molecular dynamic simulations in the *NPT* ensemble for a single thermodynamic state (in this case $T = 323.15$ K and $P = 40$ MPa). Details of the simulations are given in Section 3. Models with a range of bond lengths (a set of five values) are simulated and the optimal separation is obtained by linear interpolation to reproduce the experimental liquid density at this condition. The bond length obtained using this procedure is also reported in the footnote of Table 2. As we have already mentioned the other parameters are determined using the theory, so that the only adjustable parameter for this model is the bond length.

A more sophisticated SAFT-γ CG force field can be developed in a similar fashion by fusing together the three-segment ring model of benzene and the three-segment chain model of *n*-decane [see Figure 1(e)]. This model allows one to account for properties of the fluid that are sensitive to features of the planar geometry of the phenyl group. Unfortunately, in this particular instance we cannot make use of the SAFT-γ EoS [40] to estimate the value of the unlike attractive energy between the phenyl and alkyl groups because the group contribution theory was not specifically developed to treat ring-like groups. Instead we resort to a simple geometric combining rule for the unlike attractive interaction. The bond length is then obtained by employing the same procedure as for the simpler model of *n*-decylbenzene. The values of the parameters are provided in Table 3.

Table 2. Optimized hetero-group SAFT-γ CG Mie force field for *n*-decylbenzene developed in our work, formed by fusing the three-segment chain model for *n*-decane and the single-segment model of benzene [see Figure 1(d)]. The four parameters that characterize the segment–segment interaction are: the Mie potential energy well depth ϵ, the diameter of the segment σ, and the repulsive and attractive Mie exponents, λ_r and λ_a, respectively. *A* and *B* represent the alkyl groups of *n*-decylbenzene and the benzene group, respectively. Simple combining rules are employed for the unlike diameter and unlike repulsive exponent: $\sigma_{AB}=(\sigma_{AA}+\sigma_{BB})/2$ and $(\lambda_{r,AB}-3)=[(\lambda_{r,AA}-3)(\lambda_{r,BB}-3)]^{1/2}$.

Like parameters		Unlike parameters[a]	
$\sigma_{AA}=4.629$ Å	$\lambda_{r,AA}=19.61$	$\sigma_{AB}=4.961$ Å	$\lambda_{r,AB}=24.95$
$\epsilon_{AA}/k_B=414.90$ K	$\lambda_{a,AA}=6.00$	$\epsilon_{AB}/k_B=512.21$ K	$\lambda_{a,AB}=6.00$
$\sigma_{BB}=5.293$ Å	$\lambda_{r,BB}=32.00$		
$\epsilon_{BB}/k_B=658.17$ K	$\lambda_{a,BB}=6.00$		

[a]The bond length between the benzene segment and the first segment of the *n*-decane model is constrained to a constant value of $l_{AB}=0.681\sigma_{AB}$.

Table 3. Optimized hetero-group SAFT-γ CG Mie parameters for the *n*-decylbenzene developed in our work, formed by fusing the three-segment chain model for *n*-decane and the three-segment ring model of benzene [see Figure 1(e)]. The four parameters that characterize the segment–segment interactions are: the Mie potential energy well depth ϵ, the diameter of the segment σ, and the repulsive and attractive Mie exponents, λ_r and λ_a, respectively. *A* and *B* represent the alkyl groups and benzene groups of *n*-decylbenzene, respectively. Simple combining rules are employed for the unlike diameter, unlike energy well depth, and unlike repulsive exponent: $\sigma_{AB}=(\sigma_{AA}+\sigma_{BB})/2$, $\epsilon_{AB}=(\epsilon_{AA}\epsilon_{BB})^{1/2}$ and $(\lambda_{r,AB}-3)=[(\lambda_{r,AA}-3)(\lambda_{r,BB}-3)]^{1/2}$.

Like parameters		Unlike parameters[a]	
$\sigma_{AA}=4.629$ Å	$\lambda_{r,AA}=19.61$	$\sigma_{AB}=4.060$ Å	$\lambda_{r,AB}=14.94$
$\epsilon_{AA}/k_B=414.90$ K	$\lambda_{a,AA}=6.00$	$\epsilon_{AB}/k_B=327.354$ K	$\lambda_{a,AB}=6.00$
$\sigma_{BB}=3.490$ Å	$\lambda_{r,BB}=11.58$		
$\epsilon_{BB}/k_B=258.28$ K	$\lambda_{a,BB}=6.00$		

[a]The bond length between the first segment of the ring model of benzene and the first segment of the *n*-decane model is constrained to a constant value of $l_{AB}=0.536\sigma_{AB}$.

3. Molecular simulation details

3.1. *CG simulations*

Direct simulations of the fluid phase equilibria and single phase properties using the SAFT-γ force fields are carried out using molecular dynamics (MD) in the canonical (NVT) and isobaric–isothermal (NPT) ensembles, respectively. To keep the temperature and pressure constant during the simulation, the Nosé–Hoover thermostat [77,78] and the Melchiona *et al.* [79] modification of the Nosé–Hoover barostat are used. In all cases a potential cut-off which is six times larger than the diameter of the largest segment is used. In the model of *n*-decylbenzene formed by fusing together the single-segment model of benzene and the three-segment chain model of *n*-decane, the bond length is constrained to a constant value using the SHAKE algorithm [80]. This constraining procedure is impractical to implement for the model of *n*-decylbenzene based on the (rigid) three-segment ring model of benzene fused to the three-segment chain model of *n*-decane, and a harmonic spring is used instead to fuse the two models; we find that a spring constant of $k_s/k_B=21{,}182$ KÅ^{-2} is large enough to keep the bond length essentially constant. The number of molecules employed in our fluid phase equilibrium simulations for the single-segment and three-segment SAFT-γ CG models of benzene are $N=2592$ and $N=864$, respectively, and $N=1024$ particles are used for the single phase simulations. The equations of motion are solved using the leap-frog algorithm with a time step of 1.5 fs in the simulations of the fluid phase equilibria, and with a time step of 0.75 fs for the simulations involving single phases. All of the simulations are carried out using the DL_POLY package, version 2.0 [81].

In order to determine the fluid phase equilibria, the simulations explicitly include the vapour–liquid interface [82–84]. This methodology has been applied in numerous studies providing an equivalent description of the phase equilibrium properties obtained with other common methods such as Gibbs ensemble Monte Carlo (GEMC) [85]. The direct MD method offers a

particular advantage when low-temperature states are examined, conditions at which grand-canonical or GEMC simulations become highly inefficient owing to the low probability of insertions of particles at high densities [84,86–89]. In our molecular simulations, the systems are arranged in orthorhombic simulation boxes of constant volume $V = L_x \times L_y \times L_z$ (L being the Cartesian box lengths) with standard periodic boundary conditions [90,91]. To promote the formation of the vapour–liquid interface, the overall density of the system is taken such that the thermodynamic state lies inside the two-phase region. The simulations are then performed in the canonical ensemble by keeping the number of particles, the system volume and the temperature fixed. If the box dimensions are chosen such that $L_x = L_y = L < L_z$, where the z dimension is taken to be at least three times that in the x and y dimensions, the system will eventually form a liquid slab with two planar interfaces along the z direction in order to minimize the interfacial area. After the system reaches equilibrium, the properties of the coexisting vapour and liquid phases can be obtained as appropriate averages. A total of 2.5×10^5 time steps are used to equilibrate the system, followed by 1.0×10^6 time steps to collect ensemble averages. Statistical uncertainties are determined by performing three independent simulations for each thermodynamic state.

The vapour pressure P_v and vapour–liquid interfacial tension γ are obtained using the diagonal components of the pressure tensor $\mathbf{P}$, where the equilibrium pressure corresponds to the normal component $P_v = P_{zz}$, and the tension is related to the difference between the normal and (average) tangential components in the case of planar symmetry [92–94]:

$$\gamma = \frac{1}{2} L_z \left[P_{zz} - \frac{1}{2}\left(P_{xx} + P_{yy}\right) \right], \tag{10}$$

where the factor of two denotes the presence of two interfaces. The vapour pressure P_v can also been obtained by running a single phase simulation in the NVT ensemble using the coexisting vapour density. The test area (TA) simulation technique [95] may offer some advantages in the case of steeply repulsive potentials or large multifunctional molecules, but it was not necessary to follow this approach for the molecules studied in the current work. The coexisting vapour ρ_v and liquid ρ_l densities are obtained directly from the averages of the density profile $\rho(z)$ in the corresponding bulk regions.

The critical temperature T_c is obtained by correlating the simulation data to a Wegner expansion up to the first-order correction term [96,97],

$$\rho_l - \rho_v = B_0 |\tau|^{\beta_c} + B_1 |\tau|^{\beta_c + \Delta}, \tag{11}$$

where $\tau = 1 - T/T_c$, $\beta_c = 0.325$ is the critical exponent which is fixed at its universal renormalization-group value, Δ is the so-called gap-exponent which takes the value of 0.51, and B_i are the correction amplitudes obtained from the correlation. Once the critical temperature is known, the critical density ρ_c and critical pressure P_c are obtained from the law of rectilinear diameters and the Clausius–Clapeyron equation, respectively:

$$\frac{\rho_l + \rho_v}{2} = \rho_c + D|\tau| \tag{12}$$

and

$$\ln P = E + F/T, \tag{13}$$

where D, E and F are correlation parameters.

3.2. *Atomistic simulations*

Fully atomistic simulations of benzene are also carried out for comparative purposes in the NVT ensemble using the Nosé–Hoover thermostat [77,78]. The all-atom CHARMM27 [98] force field is used with the van der Waals interactions truncated at 15 Å. The equations of motion are solved using the leap-frog algorithm with a time step of 1 fs. The simulation cell consists of $N = 500$ benzene molecules in a cubic box with standard periodic boundary conditions. The Ewald summation method [90] is employed to handle the Coulombic interactions. The simulations for the atomistic system are also carried out using the DL_POLY package [81].

4. Results

The results of the MD simulations for the temperature–density coexistence envelope, vapour pressure curve (including the Clausius–Clapeyron representation which highlights the low temperature region), and vapour–liquid surface tension of the single-segment and refined three-segment ring SAFT-γ CG models of benzene (see Table 2) are presented in Figures 2–5. The simulated fluid phase equilibrium data are compared with the corresponding values obtained with the TraPPE UA force field [99], and the experimental data from NIST [59]. In order to quantify the quality of the predictions of the SAFT-γ models with respect to the N_{exp} experimental values, we use the average absolute deviation AAD%,

$$\text{AAD\%} = \frac{1}{N_{exp}} \sum_{i=1}^{N_{exp}} |(X_i^{exp} - X_i^{sim})/X_i^{exp}| \times 100, \tag{14}$$

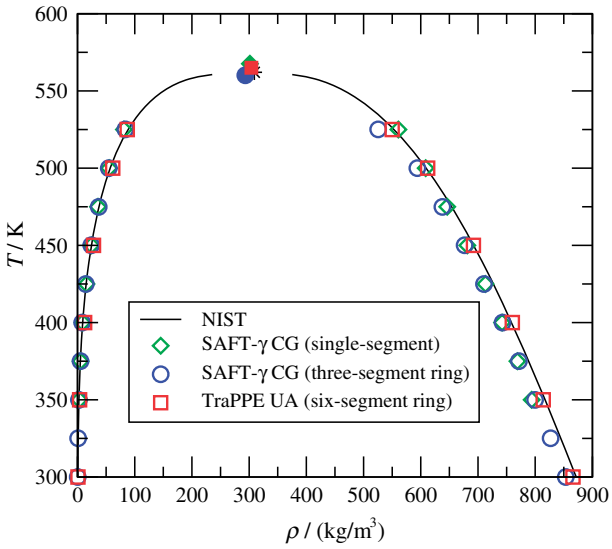

Figure 2. Temperature–density vapour–liquid coexistence curve for benzene. The continuous curves denote the smoothed experimental data from NIST [59], the diamonds and circles are the results obtained by molecular dynamics simulation using the SAFT-γ CG force field (this work) for the single-segment and three-segment ring models, respectively (see Table 1), and the squares are the corresponding data for the six-segment TraPPE UA force field [99]. The star represents the experimental critical point, while filled symbols represent the critical points obtained for the different force fields. The error bars of the data are smaller than the size of the symbols.

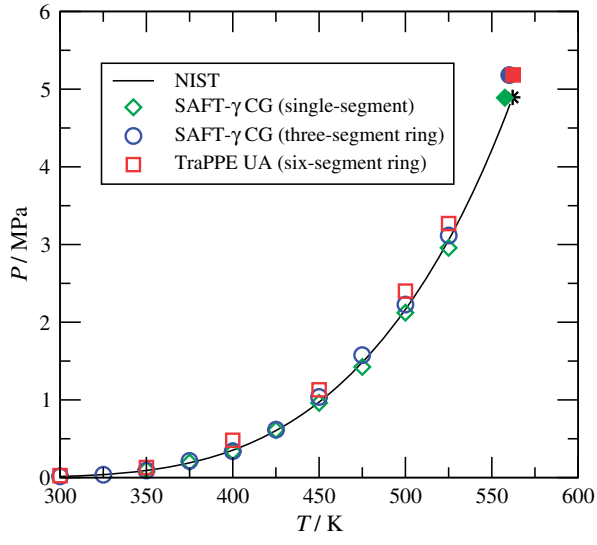

Figure 3. Vapour pressure as a function of temperature for benzene. Legend as in Figure 2.

where X_i^{exp} and X_i^{sim} are the experimental and simulated properties, respectively. As can be observed in Figure 2 our single-segment model of benzene [cf. Figure 1(a)] provides a good description of the

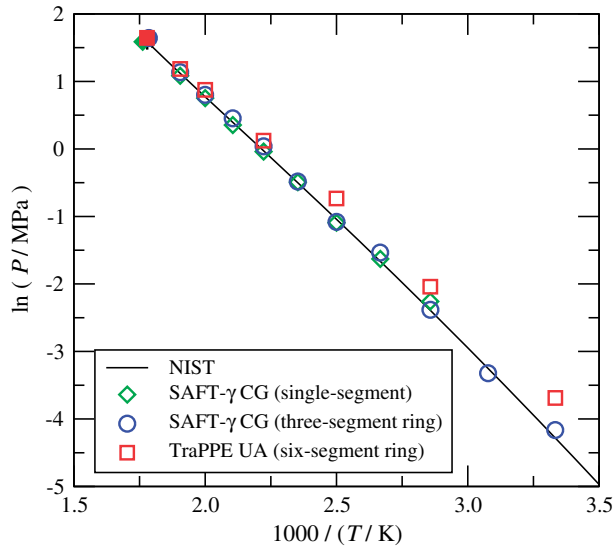

Figure 4. Vapour pressure in the Clausius–Clapeyron representation for benzene. Legend as in Figure 2.

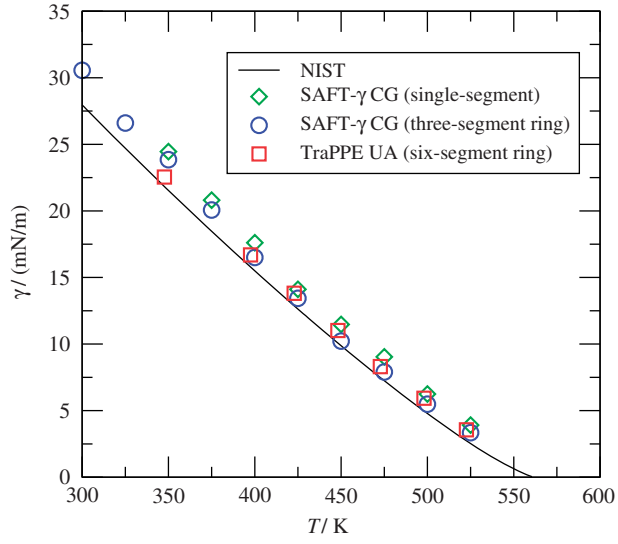

Figure 5. Vapour–liquid surface tension as a function of temperature for benzene. The data for the surface tension of the the TraPPE UA force field are taken from [100]. Legend as in Figure 2.

coexisting densities for temperatures below the critical point, with an AAD% of 1.71% for the saturated liquid densities, and of 5.98% for the saturated vapour densities over the temperature range of 350–525 K. The critical temperature and critical density obtained with this model is $T_c = 567.58 \pm 4.73$ K and $\rho_c = 301.25 \pm 0.72\,\text{kg m}^{-3}$, while the corresponding experimental values are 562.16 K and $301.58\,\text{kg m}^{-3}$, respectively. The overestimation of the critical

temperature is reflected in the behaviour of the vapour–liquid surface tension, where the shift between the simulated data for the single-segment model and the experimental values is of the same order of magnitude as the deviation in the critical temperature (cf. Figure 5). This single-segment model provides a very good representation of the vapour pressure over the entire fluid range of temperatures (cf. Figures 3 and 4), with an AAD% of 4.22%. The critical value of the vapour pressure for this model is $P_c = 4.89 \pm 0.49$ MPa; the corresponding experimental value is 4.74 MPa. It is important to stress that one is not able to capture both the coexistence curve and the saturation pressure of benzene with a single-segment 12–6 Lennard-Jones potential unless temperature-dependent molecular parameters are introduced [101]. We should also note that although our single-segment model reproduces the fluid phase behaviour well away from the critical point, the fluid tends to freeze at temperatures higher than the experimental triple point (between 350 and 375 K) as a consequence of the large value of the repulsive exponent of the CG interaction. This large value is needed to obtain a good description of the vapour pressure with the single-segment model.

By contrast, the three-segment ring SAFT-γ CG force field provides an excellent representation of the fluid phase equilibria of benzene over the entire range of temperatures as can be seen in Figures 2–5. The AAD%s for the coexisting vapour and liquid densities, and vapour pressure obtained with our ring model over a temperature range of 300–525 K are 6.13%, 2.28%, and 5.75%, respectively. The critical point obtained for this model is: $T_c = 560.06 \pm 4.45$ K, $\rho_c = 293.31 \pm 4.22$ kg m^{-3}, and $P_c = 5.18 \pm 0.31$ MPa. The description obtained with this SAFT-γ CG force field is in very good agreement with the corresponding results for the more sophisticated united-atom models such as the six-segment TraPPE UA force field [99], with a notable improvement in the description of the vapour pressure with the SAFT-γ force field: the AAD%s for the coexisting vapour and liquid densities, and vapour pressure obtained with the TraPPE UA model over the temperature range of 300–525 K are 23.89%, 0.78%, and 22.95%, respectively. Our model, however, leads to a small overshoot of the vapour–liquid surface tension curve by a constant shift; as for the single-segment model, this difference is a consequence of the slight overestimation of the critical temperature, which in this case is about 0.21%. The same deviation is observed with the TraPPE UA force field, where a small overestimation of the critical temperature is found [99,100]. The value of the repulsive exponent is smaller for the three-segment ring model than for the one-segment model, i.e., the segments are softer in comparison, allowing one to explore lower-temperature fluid states than with the single-segment model without the system freezing prematurely. A similar feature is observed with the force field developed for benzene by DeVane *et al.* [47], where the segments of their four-segment ring model interact via a soft Mie 9–6 potential (which is softer than the Lennard-Jones 12–6 potential).

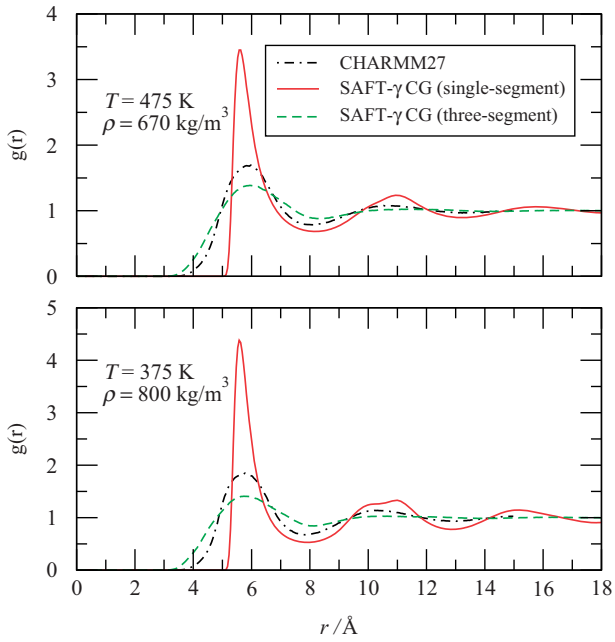

Figure 6. Centre-of-mass pair distribution functions $g(r)$ obtained for the single-segment and three-segment SAFT-γ CG models for two different thermodynamic states: (upper panel) $T = 475$ K and $\rho = 670$ kg m^{-3}; (lower panel) $T = 375$ K and $\rho = 800$ kg m^{-3}. In both cases, the results are compared with the corresponding pair distribution functions obtained using the all-atom CHARMM27 [98] force field.

As has been mentioned earlier, our SAFT-γ CG models are parametrized using experimental fluid phase equilibrium data, i.e., the models are developed to provide an optimal representation of the saturated liquid densities and vapour pressures. Arguments can be put forward to suggest that it is unlikely that a CG model would be capable of describing both the structural and thermodynamic properties with the same degree of accuracy [102,103]. For this reason one may expect that our models would not reproduce the structure of liquid benzene. In order to assess this point, the centre-of-mass radial pair distribution function $g(r)$ of liquid benzene determined at two different thermodynamic states using the SAFT-γ CG models are compared with those obtained with the all-atom CHARMM27 [98] force field in Figure 6. The densities of the two states are chosen to be close to the saturation values at the corresponding

temperatures: $T = 475$ K and $\rho = 670$ kg m^{-3}; $T = 375$ K and $\rho = 800$ kg m^{-3}. Although the structure of the liquid phase obtained with the CG and atomistic models are not in perfect agreement, the description is nevertheless encouraging considering the simplicity of the CG models. The two SAFT-γ CG models predict the position of the first peak roughly in the correct place, $r \sim 5.7$ Å. The amplitude of the peaks obtained with the single-segment CG model is overestimated. Unsurprisingly, however, the three-segment SAFT-γ CG model provides a better description of the overall structure. The pronounced peak seen in the $g(r)$ of the single-segment model is expected as the repulsive exponent of the potential is very large, i.e., the molecules interact through a very hard potential; the onset of freezing in this model can be seen in the shoulder which is starting to emerge in the second peak of $g(r)$ at the lower temperature. It would be possible to develop a version of the three-segment CG model, which is able to better reproduce the structure of liquid benzene, by matching simultaneously the saturated liquid density and vapour–liquid surface tension [47], instead of the saturated liquid density and vapour pressure which is the goal of the current work.

Having validated our SAFT-γ force fields for benzene, a key test is the transferability of the interaction parameters to related molecular systems. In our present study, molecules comprising a phenyl group are good candidates to test the transferability of our approach: *n*-decylbenzene (*n*-$C_{16}H_{26}$) is selected as an appropriate choice. For this purpose, a reliable model for *n*-decane is required to provide a good representation of the fluid behaviour over a wide range of thermodynamic conditions. In the second paper of this series [26] we developed a SAFT-γ CG model for *n*-decane, consisting of a linear chain formed from three tangent segments ($m_s = 3$) interacting via the Mie potential [see Figure 1(c)]. The molecular parameters for this model of *n*-decane are also reported in Table 1. The molecular simulation results of the fluid phase equilibria and interfacial tension using the SAFT-γ CG model of *n*-decane are shown in Figures 7–10 for comparison. It is clear that our force field provides an excellent representation of the vapour–liquid equilibria of *n*-decane, particularly the vapour pressure in the low-temperature region; the accuracy of the description is comparable to that with the more sophisticated models of *n*-decane, such as the SKS [104,105], NERD [106], and TraPPE [107] UA force fields which have been examined in some detail in [108]. The experimental critical temperature of *n*-decane is reproduced very well with our SAFT-γ model; it is found to be overestimated by only 0.5%.

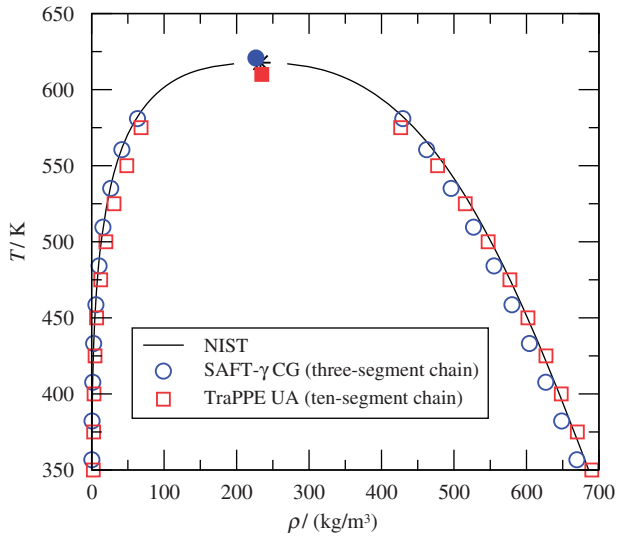

Figure 7. Temperature–density vapour–liquid coexistence curve for *n*-decane. The continuous curves denote the smoothed experimental data [59], the circles are the results obtained by molecular dynamics simulation using our SAFT-γ CG force field (see Table 1), and the squares are the results taken from [108] for the ten-segment TraPPE UA force field. The star represents the experimental critical point, while filled symbols represent the critical points obtained with the different force fields.

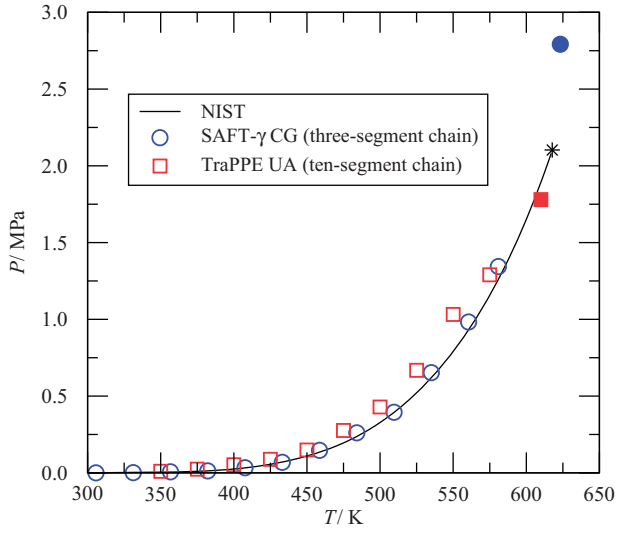

Figure 8. Vapour pressure as a function of temperature for *n*-decane. Legend as in Figure 7.

We now undertake a preliminary study of the extension of the approach to CG models of molecules formed from Mie segments of different types. Molecular dynamics simulations are carried out for several thermodynamic states in the single phase liquid

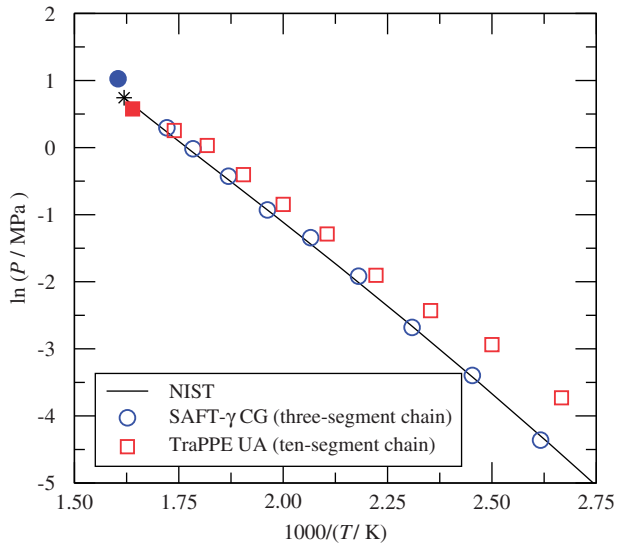

Figure 9. Vapour pressure in the Clausius–Clapeyron representation for *n*-decane. Legend as in Figure 7.

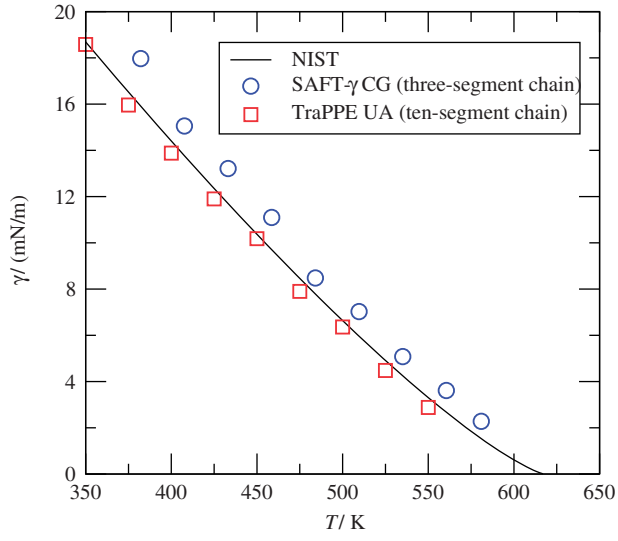

Figure 10. Vapour-liquid surface tension as a function of temperature for *n*-decane. Legend as in Figure 7.

region at subcritical temperatures for the simple single-segment phenyl hetero-group SAFT-γ CG force field of *n*-decylbenzene discussed in Section 2.2 (see Figure 1(d) and Table 2 for the values of the parameters). The temperature dependence of the liquid density for a range of pressures obtained with our model is shown in Figure 11. In the temperature range of 293–353 K for pressures above 20 MPa, the model is seen to provide a very good representation of

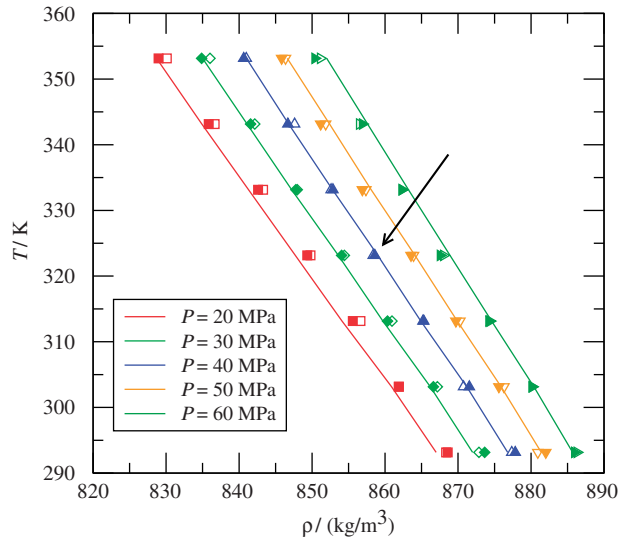

Figure 11. Temperature dependence of the liquid density of *n*-decylbenzene ($C_{16}H_{26}$) for isobars corresponding to $P = 20$, 30, 40, 50, and 60 MPa. The continuous curves denote the smoothed experimental data from [109], and the symbols are the results of the isobaric–isothermal ensemble molecular dynamics simulation for our hetero-group SAFT-γ CG Mie models of *n*-decylbenzene. The open symbols denote the values for the *n*-decylbenzene force field with the single-segment model of benzene to represent the phenyl group [see Figure 1(d)], while the filled symbols are the results using the three-segment ring model of the phenyl group [see Figure 1(e)]. The arrow denotes the thermodynamic state used for the estimation of the bond length between the phenyl and *n*-decyl groups.

the experimental data [109]. It is very encouraging to observe that our simple CG model, developed with a single adjustable bond length estimated from a single state point, allows one to reproduce the liquid density for a wide range of thermodynamic states. It is only at pressures lower than 20 MPa that the model starts to exhibit a small deviation from the experimental data. An improved SAFT-γ CG force field for *n*-decylbenzene is constructed by fusing the three-segment ring model of benzene with the three-segment chain model of *n*-decane [see Figure 1(e)]. The interaction parameters for this model are summarized in Table 3. As is apparent from Figure 11, the model with the more detailed representation of the geometry of the phenyl group allows for a better representation of the liquid density over a wide range of temperatures and pressures. This provides a preliminary indication of how the SAFT-γ methodology can be used to obtain molecular parameters for different functional groups that can then serve as building blocks for molecular models suitable for molecular simulation.

5. Conclusions

We have described the application of our SAFT-γ CG methodology to develop an accurate CG force field for the fluid phase behaviour of benzene. In our approach the SAFT-VR Mie EoS is used as the link between the experimental fluid phase data and the parameters of the CG models. The intermolecular parameters obtained in this way for models based on the Mie potential can be used over a wide range of thermodynamic conditions, as the parameters are obtained by using extensive experimental data. This procedure is very efficient since the theory is algebraic, allowing for fast calculations. Two models of benzene are developed in the current work. The first one consists of a single-segment interacting via the Mie potential. Despite the simplicity of the description, the model provides a good representation of the fluid phase behaviour of benzene for conditions away from the critical region. The vapour pressure, in particular, is very well described with this model, which results from an appropriate description of the softness/hardness of the intermolecular potential. For the second model of benzene we represent the molecule as a three-segment ring structure, formed from segments also interacting through potentials of the Mie form. The latter model is more realistic as it preserves some features of the planar geometry characteristic of benzene. The fluid phase behaviour of benzene obtained with this SAFT-γ CG force field is of comparable accuracy to that obtained with more sophisticated united atom models commonly employed in the field. It is also very gratifying to find that the structure of the fluid is represented reasonably well with this model.

In this work, we have also developed hetero-group SAFT-γ models for the fluid phase behaviour of *n*-decylbenzene. The phenyl and *n*-decyl groups in this molecule are described with the individual models for benzene (single-segment and three-segment ring) developed in the current work and with our previously reported model of *n*-decane, respectively. This is the first example of a hetero-group model developed with our SAFT-γ methodology. It is very encouraging to find that the intermolecular parameters can be transferred in an effective manner from the groups obtained for simpler molecules such as benzene and the *n*-alkanes to construct the more complex alkylbenzenes. The liquid phase of *n*-decylbenzene is accurately represented over a wide range of thermodynamic conditions without the need for an extensive parameter estimation procedure. In future work, the version of the SAFT-γ group contribution EoS based on Mie segments [40] will be used in order to develop SAFT-γ force field parameters for a wide range of united atom functional groups. Here we have demonstrated the methodology for models formed from tangent segments. In forthcoming work we will show that the distance between the segments (bond length) can also be estimated using the theory.

Acknowledgements

C.A. and T.L. are very grateful to the Engineering and Physical Sciences Research Council (EPSRC) of the UK for the award of postdoctoral fellowships. Additional funding to the Molecular Systems Engineering Group from the EPSRC (grants GR/T17595, GR/N35991, and EP/E016340), the Joint Research Equipment Initiative (JREI) (GR/M94426), and the Royal Society-Wolfson Foundation refurbishment scheme is also gratefully acknowledged. The simulations were performed using the facilities of the Imperial College High Performance Computing Service.

References

[1] W.G. Noid, J.-W. Chu, G.S. Ayton, V. Krishna, S. Izvekov, G.A. Voth, A. Das and H.C. Andersen, J. Chem. Phys. **128**, 244114 (2008).
[2] K.E. Gubbins and J.D. Moore, Ind. Eng. Chem. Res. **49**, 3026 (2010).
[3] F. Müller-Plathe, Chem. Phys. Chem. **3**, 754 (2002).
[4] S.O. Nielsen, C.F. López, G. Srinivas and M.L. Klein, J. Phys. Condens. Matter **16**, R481 (2004).
[5] R. Faller, Phys. Chem. Chem. Phys. **11**, 1867 (2009).
[6] C. Peter and K. Kremer, Soft Matter **5**, 4357 (2009).
[7] G.A. Voth, *Coarse-Graining of Condensed Phase and Biomolecular Systems* (CRC Press, New York, 2009).
[8] C. Peter and K. Kremer, Faraday Discuss. **144**, 9 (2010).
[9] A.P. Lyubartsev and A. Laaksonen, Phys. Rev. E **52**, 3730 (1995).
[10] D. Reith, M. Pütz and F. Müller-Plathe, J. Comput. Chem. **24**, 1624 (2003).
[11] S. Izvekov, M. Parrinello, C.J. Burnham and G.A. Voth, J. Chem. Phys. **120**, 10896 (2004).
[12] S. Izvekov and G.A. Voth, J. Chem. Phys. **123**, 134105 (2005).
[13] S. Izvekov and G.A. Voth, J. Phys. Chem. B **109**, 2469 (2005).
[14] S.J. Marrink, H.J. Risselada, S. Yefimov, D.P. Tieleman and A.H. de Vries, J. Phys. Chem. B **111**, 7812 (2007).
[15] J.C. Shelley, M.Y. Shelley, R.C. Reeder, S. Bandyopadhyay and M.L. Klein, J. Phys. Chem. B **105**, 4464 (2001).
[16] S.O. Nielsen, C.F. Lopez, G. Srinivas and M.L. Klein, J. Chem. Phys. **119**, 7043 (2003).
[17] W. Shinoda, R. DeVane and M.L. Klein, Mol. Simul. **33**, 27 (2007).
[18] R. DeVane, W. Shinoda, P.B. Moore and M.L. Klein, J. Chem. Theory Comput. **5**, 2115 (2009).
[19] J.E. Jones, Proc. R. Soc. London A **106**, 463 (1924).

[20] J.E. Lennard-Jones, Proc. Phys. Soc. London **43**, 461 (1931).
[21] G. Mie, Ann. Phys. **316**, 657 (1903).
[22] K.A. Maerzke and J.I. Siepmann, J. Phys. Chem. B **115**, 3452 (2011).
[23] W.G. Chapman, K.E. Gubbins, G. Jackson and M. Radosz, Fluid Phase Equilib. **52**, 31 (1989).
[24] W.G. Chapman, K.E. Gubbins, G. Jackson and M. Radosz, Ind. Eng. Chem. Res. **29**, 1709 (1990).
[25] C. Avendaño, T. Lafitte, A. Galindo, C.S. Adjiman, G. Jackson and E.A. Müller, J. Phys. Chem. B **115**, 11154 (2011).
[26] C. Avendaño, T. Lafitte, A. Galindo, C.S. Adjiman, E.A. Müller and G. Jackson, J. Phys. Chem. B, submitted (2012).
[27] E.A. Müller and K.E. Gubbins, Ind. Eng. Chem. Res. **40**, 2193 (2001).
[28] I.G. Economou, Ind. Eng. Chem. Res. **41**, 953 (2002).
[29] S.P. Tan, H. Adidharma and M. Radosz, Ind. Eng. Chem. Res. **47**, 8063 (2008).
[30] C. McCabe and A. Galindo, in *Applied Thermodynamics of Fluids*, edited by A. Goodwin, J.V. Sengers, and C.J. Peters (Royal Society of Chemistry, UK, 2010).
[31] A. Gil-Villegas, A. Galindo, P.J. Whitehead, S.J. Mills, G. Jackson and A.N. Burgess, J. Chem. Phys. **106**, 4168 (1997).
[32] A. Galindo, L.A. Davies, A. Gil-Villegas and G Jackson, Mol. Phys. **93**, 241 (1998).
[33] L.A. Davies, A. Gil-Villegas and G. Jackson, Int. J. Thermophys. **19**, 675 (1998).
[34] L.A. Davies, A. Gil-Villegas and G. Jackson, J. Chem. Phys. **111**, 8659 (1999).
[35] T. Lafitte, B. Bessieres, M.M. Piñeiro and J.-L. Daridon, J. Chem. Phys. **124**, 024509 (2006).
[36] T. Lafitte, A. Apostolakou, C. Avendaño, A. Galindo, C.S. Adjiman, E.A. Müller and G. Jackson, in preparation (2012).
[37] A. Lymperiadis, C.S. Adjiman, A. Galindo and G. Jackson, J. Chem. Phys. **127**, 234903 (2007).
[38] A. Lymperiadis, C.S. Adjiman, G. Jackson and A. Galindo, Fluid Phase Equilib. **274**, 85 (2008).
[39] V. Papaioannou, C.S. Adjiman, G. Jackson and A. Galindo, Fluid Phase Equilib. **306**, 82 (2011).
[40] V. Papaioannou, T. Lafitte, C. Avendaño, C.S. Adjiman, G. Jackson, E.A. Müller and A. Galindo, in preparation (2012).
[41] C.A. Hunter and J.K.M. Sanders, J. Am. Chem. Soc. **112**, 5525 (1990).
[42] C.A. Hunter, K.R. Lawson, J. Perkins and C.J. Urch, J. Chem. Soc., Perkin Trans. 2, 651 (2001).
[43] W.L. Jorgensen, J.D. Madura and C.J. Swenson, J. Am. Chem. Soc. **106**, 6638 (1984).
[44] W.L. Jorgensen and D.L. Severance, J. Am. Chem. Soc. **112**, 4768 (1990).
[45] N. Zacharopoulos, N. Vergadou and D.N. Theodorou, J. Chem. Phys. **122**, 244111 (2005).
[46] H. Sun, J. Phys. Chem. B **102**, 7338 (1998).
[47] R. DeVane, M.L. Klein, C.-C. Chiu, S.O. Nielsen, W. Shinoda and P.B. Moore, J. Phys. Chem. B **114**, 6386 (2010).
[48] M.S. Wertheim, J. Stat. Phys. **35**, 19 (1984).
[49] M.S. Wertheim, J. Stat. Phys. **35**, 35 (1984).
[50] M.S. Wertheim, J. Stat. Phys. **42**, 459 (1986).
[51] M.S. Wertheim, J. Stat. Phys. **42**, 477 (1986).
[52] W.G. Chapman, G. Jackson and K.E. Gubbins, Mol. Phys. **65**, 1057 (1988).
[53] P. Paricaud, S. Varga and G. Jackson, J. Chem. Phys. **118**, 8525 (2003).
[54] R.P. Sear and G. Jackson, Mol. Phys. **81**, 801 (1994).
[55] R.P. Sear and G. Jackson, Phys. Rev. E **50**, 386 (1994).
[56] D. Ghonasgi and W.G. Chapman, J. Chem. Phys. **102**, 2585 (1995).
[57] R.P. Sear and G. Jackson, Mol. Phys. **87**, 517 (1996).
[58] T. van Westen, T.J.H. Vlugt and J. Gross, J. Phys. Chem. B **115**, 7872 (2011).
[59] E.W. Lemmon, M.O. McLinden and D.G. Friend, *NIST Chemistry Webbook, NIST Standard Reference Database, Number 69* (National Institute of Standards and Technology, Gaithersburg MD). http://webbook.nist.gov/
[60] F. London, Trans. Faraday Soc. **33**, 8 (1937).
[61] A.L. Archer and G. Jackson, Mol. Phys. **73**, 881 (1991).
[62] M.D. Amos and G. Jackson, Mol. Phys. **74**, 191 (1991).
[63] R.P. Sear, M.D. Amos and G. Jackson, Mol. Phys **80**, 777 (1993).
[64] M.D. Amos and G. Jackson, J. Chem. Phys. **96**, 4604 (1992).
[65] A.L. Archer, M.D. Amos, G. Jackson and I.A. McLure, Int. J. Thermophys. **17**, 201 (1996).
[66] H. Adidharma and M. Radosz, Ind. Eng. Chem. Res. **37**, 4453 (1998).
[67] C. McCabe, A. Gil-Villegas, G. Jackson and F. del Río, Mol. Phys. **97**, 551 (1999).
[68] Y. Peng, H. Zhao and C. McCabe, Mol. Phys. **104**, 571 (2006).
[69] H. Adidharma and M. Radosz, Fluid Phase Equilib. **158**, 165 (1999).
[70] P. Morgado, H. Zhao, F.J. Blas, C. McCabe, L.P.N. Rebelo and E.J.M. Filipe, J. Phys. Chem. B **111**, 2856 (2007).
[71] M. Banaszak, C.K. Chen and M. Radosz, Macromolecules **29**, 6481 (1996).
[72] F.J. Blas and L.F. Vega, Mol. Phys. **92**, 135 (1997).
[73] M. Banaszak and M. Radosz, Fluid Phase Equilib. **193**, 179 (2002).
[74] J. Gross, O. Spuhl, F. Tumakaka and G. Sadowski, Ind. Eng. Chem. Res. **42**, 1266 (2003).
[75] Y. Peng, K.D. Goff, M.C. dos Ramos and C. McCabe, Fluid Phase Equilib. **277**, 131 (2009).
[76] Y. Peng, K.D. Goff, M.C. dos Ramos and C. McCabe, Ind. Eng. Chem. Res. **49**, 1378 (2010).
[77] S. Nosé, J. Chem. Phys. **81**, 511 (1984).
[78] W.G. Hoover, Phys. Rev. A **31**, 1695 (1985).
[79] S. Melchionna, G. Ciccotti and B.L. Holian, Mol. Phys. **78**, 533 (1993).

[80] J.P. Ryckaert, G. Ciccotti and H.J.C. Berendsen, J. Comput. Phys. **23**, 327 (1977).
[81] W. Smith, Mol. Simul. **32**, 933 (2006).
[82] G.A. Chapela, G. Saville and J.S. Rowlinson, Faraday Discuss. **59**, 22 (1975).
[83] G.A. Chapela, G. Saville, S.M. Thompson and J.S. Rowlinson, J. Chem Soc., Faraday Trans. **73**, 1133 (1977).
[84] F. Martínez-Veracoechea and E.A. Müller, Mol. Simul. **31**, 33 (2005).
[85] A.Z. Panagiotopoulos, Mol. Phys. **61**, 813 (1987).
[86] A. Trokhymchuk and J. Alejandre, J. Chem. Phys. **111**, 8510 (1999).
[87] L.D. Gelb and E.A. Müller, Fluid Phase Equilib. **203**, 1 (2002).
[88] E.G. Noya, C. Vega and E. de Miguel, J. Chem. Phys. **128**, 154507 (2008).
[89] E.A. Müller and A. Mejía, Fluid Phase Equilib. **282**, 68 (2009).
[90] M.P. Allen and D.J. Tildesley, *Computer Simulation of Liquids* (Oxford University Press, Oxford, 1987).
[91] D. Frenkel and B. Smit, *Understanding Molecular Simulation*, 2nd ed. (Academic Press, London, 2002).
[92] J.S. Rowlinson and B. Widom, *Molecular Theory of Capillarity* (Clarendon, Oxford, 1982).
[93] E. de Miguel and G. Jackson, J. Chem. Phys. **125**, 164109 (2006).
[94] E. de Miguel and G. Jackson, Mol. Phys. **104**, 3717 (2006).
[95] G.J. Gloor, G. Jackson, F.J. Blas and E. de Miguel, J. Chem. Phys. **123**, 134703 (2005).
[96] F.J. Wegner, Phys. Rev. B **5**, 4529 (1972).
[97] L. Vega, E. de Miguel, L.F. Rull, G. Jackson and I.A. McLure, J. Chem. Phys. **96**, 2296 (1992).
[98] A.D. MacKerell, D. Bashford, M. Bellott, R.L. Dunbrack, J.D. Evanseck, M.J. Field, S. Fischer, J. Gao, H. Guo, S. Ha, D. Joseph-McCarthy, L. Kuchnir, K. Kuczera, F.T.K. Lau, C. Mattos, S. Michnick, T. Ngo, D.T. Nguyen, B. Prodhom, W.E. Reiher, B. Roux, M. Schlenkrich, J.C. Smith, R. Stote, J. Straub, M. Watanabe, J. Wiorkiewicz-Kuczera, D. Yin and M. Karplus, J. Phys. Chem. B **102**, 3586 (1998).
[99] C.D. Wick, M.G. Martin and J.I. Siepmann, J. Phys. Chem. B **104**, 8008 (2000).
[100] J. Janeček, H. Krienke and G. Schmeer, Condens. Matter Phys. **10**, 415 (2007).
[101] E.A. Müller and L.D. Gelb, Ind. Eng. Chem. Res. **42**, 4123 (2003).
[102] H. Wang, C. Junghans and K. Kremer, Eur. Phys. J. E **28**, 221 (2009).
[103] A.A. Louis, comment in Faraday Discuss. **144**, 323 (2010).
[104] B. Smit, S. Karaborni and J.I. Siepmann, J. Chem. Phys. **102**, 2126 (1995).
[105] B. Smit, S. Karaborni and J.I. Siepmann, J. Chem. Phys. **109**, 352 (1998).
[106] S.K. Nath, F.A. Escobedo and J.J. de Pablo, J. Chem. Phys. **108**, 9905 (1998).
[107] M.G. Martin and J.I. Siepmann, J. Phys. Chem. B **102**, 2569 (1998).
[108] E.A. Müller and A. Mejía, J. Phys. Chem. B **115**, 12822 (2011).
[109] M. Milhet, A. Baylaucq and C. Boned, J. Chem. Eng. Data **50**, 1430 (2005).